THERMOELECTRICAL PROPERTIES OF POLITHIOPHENE (P3HT) THIN FILM POLYMERS

by

İbrahim Gökhan Hacıahmetoğlu

B.S., Electrical and Electronics Engineering, Boğaziçi University, 2010

Submitted to the Institute for Graduate Studies in
Science and Engineering in partial fulfillment of
the requirements for the degree of
Master of Science

Graduate Program in Electrical and Electronics Engineering Department
Boğaziçi University

2013

ACKNOWLEDGEMENTS

My deepest appreciation belongs to my thesis supervisor Assoc. Prof. Şenol Mutlu for his encouragements, comments and suggestions. Without his guidance and excitement in researching and teaching, this thesis would not have been possible. I would also like to thank Assoc. Prof. Hakan Ertürk and Assist. Prof. Hamdi Torun for their help, and suggestions.

I would like to thank all of my friends for their friendships, funny talks and leisure activities. Especially I would like to mention İsmail Terkeşli, Vahap Barış Esen, İsmail Kara, Berkan Yaman and, Bilgiday Yüce.

In addition, I would like to thank TÜBİTAK for supporting me through BİDEB scholarship program between 2010-2012.

Finally, I am most grateful to my dear parents Hanife and Orhan Hacıahmetoğlu with my brother, Hakan, for their lifelong love and supports under all circumstances.

ABSTRACT

THERMOELECTRICAL PROPERTIES OF POLITHIOPHENE (P3HT) THIN FILM POLYMERS

Conducting and semiconducting polymers show very interesting thermoelectric characteristics by having relatively high electrical but low thermal conductivity. This suggests that they can be used in thermoelectric patterning, which is achieved by forming localized and confined heated areas on the material by passing electric current through it. This thesis examines the usage of polymeric semiconductor of poly (3-hexyl thiophene)(P3HT) in thermoelectric applications. An experimental setup is build to measure the lateral thermal conductivity of P3HT thin film polymer to be 3.7 W/mK, which is not close to the reported real value of 0.2 W/mK. The analysis of measurement setup and results show significant error induced by considerable amounts of thermal paths between measurement thermal probes alternative to the thermal path through the sample. Some suggestions are made to improve the experimental setup. Effect of doping on electrical conductivity and Seebeck coefficient of P3HT is discussed to increase the thermoelectric figure of merit, ZT. ZT of P3HT is calculated with thermal conductivity value of 0.2 W/mK and found to be 2.5 x 10^{-4}.

ÖZET

POLİTİYOFEN (P3HT) İNCE POLİMER FİLMLERİN TERMOELEKTRİKSEL OZELLİKLERİ

Yarıiletken ve iletken polimerler görece yüksek elektriksel ve düşük termal iletkenlikleriyle ilgi çekici termoelektriksel özellikler gösterirler. Bu aynı zamanda termoelektrik örneklemede de kullanılabileceklerini önerir. Termoelektirk örnemkleme elektrik akımını malzemeden geçirme yoluyla ısıyı belirli bir bölgede tutmak olarak tanımlanır. Bu tez polimerik yarıiletken politiyofen (P3HT) filmin termoelektrik uygulamalardaki kullanılabilirliğini incelemektedir. Yatay termal iletkenliği ölçmek için bir deney düzeneği kuruldu ve bu değer 3.7 W/mK olarak ölçüldü ancak bu değer rapor edilen 0.2 W/mK değerinden uzaktır. Deneysel düzenek üzerinde yapılan analizler ve sonuçların gösterdiği gibi, örnekten geçen ısıya alternatif ısı iletim yolları yüksek miktarda hataya sebep olmaktadır. Deneysel düzeneği geliştirmek için bazı önerilerde bulunuldu. P3HT' nin termoelektriksel değer katsayısını yükseltmek için katkılamanın elektrik iletkenliği ve Seebeck katsayısı üzerindeki etkileri tartışıldı. P3HT'nin termoelektriksel değer katsayısı 0.2 W/mK termal iletkenlik değeri kullanılarak $2.5\text{x}10^{-4}$ olarak bulundu.

TABLE OF CONTENTS

LIST OF FIGURES

LIST OF TABLES

LIST OF SYMBOLS

C	Electrical capacitance
C_T	Thermal capacitance
F	View factor
f	Frequency
I	Electrical current
Kn	Knudsen number
P	Power
R	Electrical resistance
T	Temperature
Q	Heat
$\overrightarrow{Q}$	Heat flux
V	Electrical potential difference
W	Thermal resistance
Z	Thermoelectric figure of merit
α	Seebeck coefficient
β	Temperature coefficient of resistance
ε	Emissivity
λ	Thermal conductivity
σ	Electrical conductivity
σ	Stefan-Boltzman constant
ϕ	Efficiency
ϕ_P	Efficiency at maximum power
φ	Phase shift
ω	Frequency

LIST OF ACRONYMS/ABBREVIATIONS

AFM	Atomic Force Microscopy
Ag	Silver
Al	Aluminium
Au	Gold
Cu	Copper
DI Water	Deionized Water
DMSO	Dimethyl Sulfoxide
Fe	Iron
HOMO	Highest Occupied Molecular Orbital
LED	Light-Emitting Diode
LUMO	Lowest Unoccupied Molecular Orbital
MTR	Multiple Trapping and Release Model
P3HT	Poly (3-hexyl thiophene)
PBTTT	poly (2,5-bis (3-tetradecylthiophen-2-yl)thieno thiophene)
PEDOT:PSS	poly (3,4-ethylenedioxythiophene) poly (styrenesulfonate)
XRD	X-ray Diffraction
VRH	Variable Range Hopping

1. INTRODUCTION

Although semiconducting and conducting polymers have a short story; they have played indispensable roles in specialized industrial applications due to their semiconductivity and other fascinating properties [1]. Research on conducting and semiconducting polymers continues in many areas such as peltier coolers, thermoelectric power generators, sensors, light-emitting diodes (LEDs), secondary batteries, transistors, and photovoltaic cells [1, 2]. Unfortunately, the aging and instability even in inert environments limited the practical uses of these polymers in real-world applications.

Unique thermoelectric properties of conducting and semiconducting polymers make them promising materials in thermoelectric and thermoelectric patterning applications where thermoelectric patterning stands for thermal patterning using electric conduction. A basic schematic of thermoelectric patterning is shown is Figure 1.1. However, unlike their inorganic counterparts, thermoelectric properties of conducting and semiconducting polymers have not been thoroughly investigated [3]. Their relatively low electrical resistivity and high thermal resistivity make them suitable in some thermoelectrical applications like peltier coolers and thermoelectric power generators. Moreover; high electrical conductivity and low thermal conductivity makes them promising materials for thermoelectric patterning which is widely used in many molecular biology and chemical analysis techniques [4]. To show the uniqueness of conducting and semiconducting polymers a list of thermal and electrical conductivities of different materials is shown below in Table 1.1 [5–10].

A graph of electrical conductivity vs thermal conductivity is drawn from Table 1.1 which is shown in Figure 1.2. Materials can be grouped in 4 different categories in terms of their electrical and thermal conductivities:

- High thermal and electrical conductivity
- High thermal and low electrical conductivity
- Low thermal and high electrical conductivity

Table 1.1. List of electrical and thermal conductivities of different materials [5-10].

Material	Thermal Conductivity(W/mK)	Electrical Conductivity(S/m)
Air	2.40E-02	7.83E-15
Al	2.50E+02	3.78E+07
Stainless steel	1.60E+01	1.18E+06
Quartz fused	1.40E+00	1.00E-16
Sillicon	1.49E+02	1.20E-03
Glass	1.20E+00	1.00E-12
SU-8 Polimer	2.00E-01	1.28E-13
PVDF	1.87E-01	5.00E-13
Diamond	2.20E+03	1.00E-16
Graphite	1.20E+02	7.37E+04
Graphene	4.90E+03	1.00E+08
PEDOT:PSS	2.00E-01	1.00E+03
Pentacene	5.10E-01	1.00E+01
Bismuth	7.97E+00	7.75E+05
Ceramic	2.00E+01	5.00E-12
Poly-si	2.40E+01	1.00E+07
SiGe	4.80E+00	1.00E+07
Bi2Te3	1.50E+00	1.00E+07
PbTe	2.30E+00	1.00E+07
Fe	7.24E+01	1.16E+07
Au	3.14E+02	4.35E+07
Cu	3.98E+02	5.81E+07
Ag	4.18E+02	6.25E+07
Selenium	5.19E-01	8.33E+06
Aluminum nitride	1.80E+02	1.00E-11
Aluminum oxide	3.50E+01	1.00E-12
Carbon nanotube	3.20E+03	1.00E+08
Rubber	1.60E-01	1.00E-13

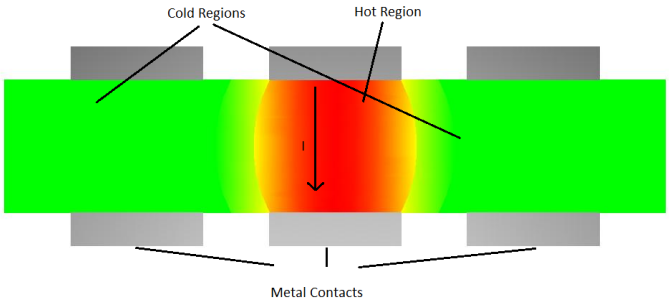

Figure 1.1. A basic schematic of thermoelectric patterning.

- Low thermal and electrical conductivity

It can easily be shown from the graph that conducting and semiconducting polymers can fill the low thermal and high electrical conductivity group. As a result, they are promising thermoelectric materials and thermoelectric properties of the conducting and semiconducting polymers should be investigated to obtain high thermoelectric figure of merit. In addition to this, conducting and semiconducting polymers are promising materials for thermoelectric patterning.

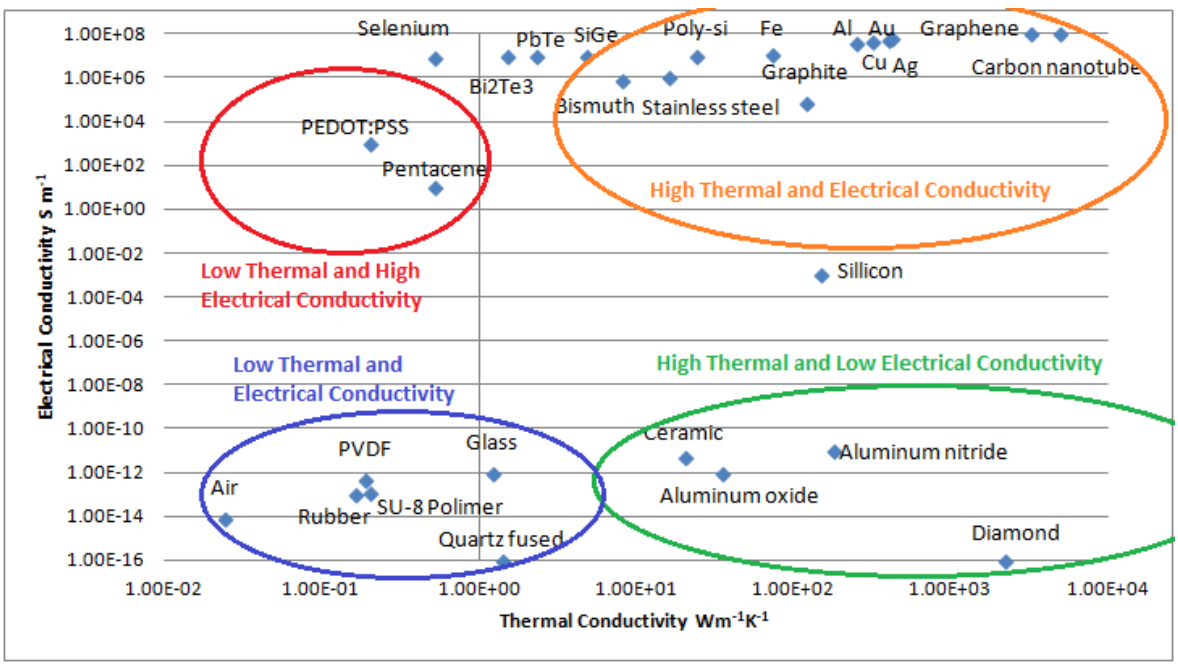

Figure 1.2. Electrical conductance vs. thermal conductance graph.

Lateral thermal conductivity of Poly (3-hexyl thiophene) (P3HT) semiconducting thin film polymer is measured because the physical properties of the P3HT thin films are anisotropic [11, 12] and suitability of P3HT is discussed for usage in thermoelectric patterning and thermoelectric field.

In this thesis, usability of P3HT in thermoelectric applications and thermoelectric patterning fields is discussed and a design of a experimental setup to measure the lateral thermal conductivity is examined because of the anisotropy of the physical properties of the conducting and semiconducting thin film polymers. Chapter 2 provides a short theoretical information about conducting and semiconducting polymers. In Chapter 3, properties of thermoelectric materials are summarized. In Chapter 4, thermoelectric properties of P3HT is discussed, the experimental setup for the thermal conductivity measurement is described, and the experimental results are given. Finally, Chapter 5 represents the conclusion and the future work.

2. CONDUCTING AND SEMICONDUCTING POLYMERS

Due to their unique chemical, mechanical, electrical, thermal, and optical properties conducting and semiconducting polymers are used in many technological areas nowadays [13]. Mechanism of charge carrier transport and the bulk heterojunctions of conducting and semiconducting polymers on atomic scale are important issues to understand the devices based on organic conductors [14, 15].

Organic semiconductors are mainly composed of C (carbon) atoms. By exciting a 2s electron into the empty 2p orbital allows the atom to make four bonds. When 2s orbitals combine with 2p orbitals four single bonds occur with other atoms which are called as σ-bonds and have highly localized electron density. Whereas; if sp2 occurs; which means the 2s orbitals is mixed with only two of the three available 2p orbitals; remaining 2p orbitals form π-bond that creates the electrical conductivity [16].

Highest occupied molecular orbitals (HOMO) are the valance bands of the conducting and semiconducting polymers. The covalent interaction increases the band gap of the conducting and semiconducting polymers by lowering HOMO. On the other hand; lowest unoccupied molecular orbitals (LUMO) are the conducting bands of the conducting and semiconducting polymers. The significant charge distribution across the interface in the ground state leads to efficient exciton dissociation even under low exciton density conditions and increases the bandgap of the conducting and semiconducting polymers [15].

2.1. Molecular Structure

The molecules that have been synthesized to use as a conducting or semiconducting polymer can be grouped in two classes in terms of their molecular structure: -solution processable polymers like poly-3(hexylthiophene) (P3HT), poly(2,5-

bis(3-tetradecylthiophen-2-yl)thieno tiophene) (PBTTT) other thiophene derivatives and small molecules typically processed in vacuum like pentacene and rubene. Molecular structures of P3HT, PBTTT, TIPS-pentacene, and rubene are shown in Figure 2.1 [17].

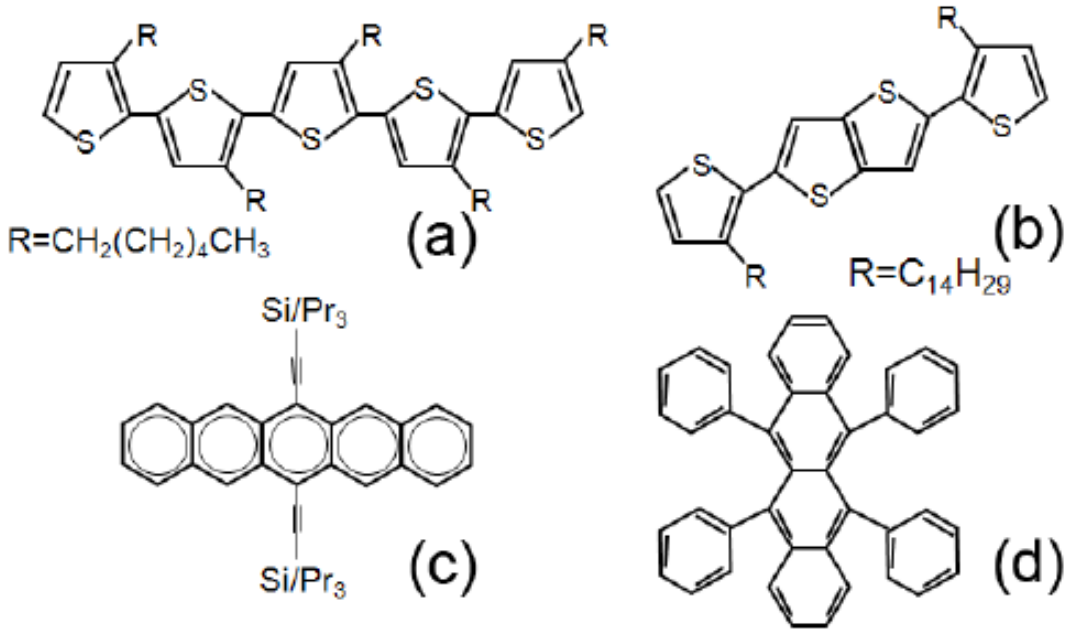

Figure 2.1. Molecular structures of (a)P3HT,(b) PBTTT, (c)TIPS-pentacene, (d)and rubene[17].

Different chemical structures change many of the properties of the materials. For instance, because of the long, conjugated backbone found in P3HT and PBTTT, these materials can undergo mechanical deformation. However, this flexibility comes with lower charge carrier mobility. P3HT and other thiophene based materials have regular ordering of repeating units to increase charge carrier mobility which is shown Figure 2.1a. With the help of the ordering of the individual P3HT units, π-band overlap between neighboring polymer chains which increases the charge carriers. On the other hand; materials like pentacene and rubrene have crystalline molecular structures which makes them rigid. However, they can exhibit high mobilities because they have long range ordering. The mobility of the organic materials P3HT, PBTTT, and pentacene lies in the range of 0.1-1 cm^2/Vs. However, the mobility of the rubene is around 15

cm^2/Vs [17].

Moreover, molecular structure causes anisotropy for P3HT films. It is shown that the P3HT structure involves two-dimensional sheets of π-stacked polythiophene backbones separated by layers of alkyl side chains from the X-ray diffraction (XRD) analysis [12]. Anisotropy is larger for semicrystalline polymers than fully amorphous polymers. An image of a directionally crystallized P3HT film can be seen in Figure 2.2 [11]. Studies show that anisotropy factor for thermal diffusivity ranges from 2 for amorphous structure to about 50 for completely crystalline polymers. From the data that is reported from various studies, lateral thermal conductivity is larger by a factor of six than the effective vertical thermal conductivity when the thickness of the thin film polymer varies between 0.5 and 2.5 μm [18].

Widely used different synthesis methods such as solvent casting and spin coating cause different crystalline orientation. For instance, in solvent casting method, needle or plate like crystallites oriented with respect to the substrate are formed. However, in spin coating method non-equilibrium structures with reduced order are formed which affects the anisotropy of the thin film [18].

2.2. Charge Transport

In organic materials the carriers need to travel over a long distance compared to conjugated molecules where carriers are transported within the molecules. Because of the reason mentioned above, the charge transport in conducting and semiconducting polymers is determined by how the carriers move between neighboring molecules [19].

In conjugated materials disorder and weak van der Waals intermolecular interactions make charge carriers to localize to a finite number of adjacent molecules, or even to individual molecules. As a result, trapping in localized states limits the charge transport in conducting and semiconducting polymers and the mobility of the polymer is activated thermally [19].

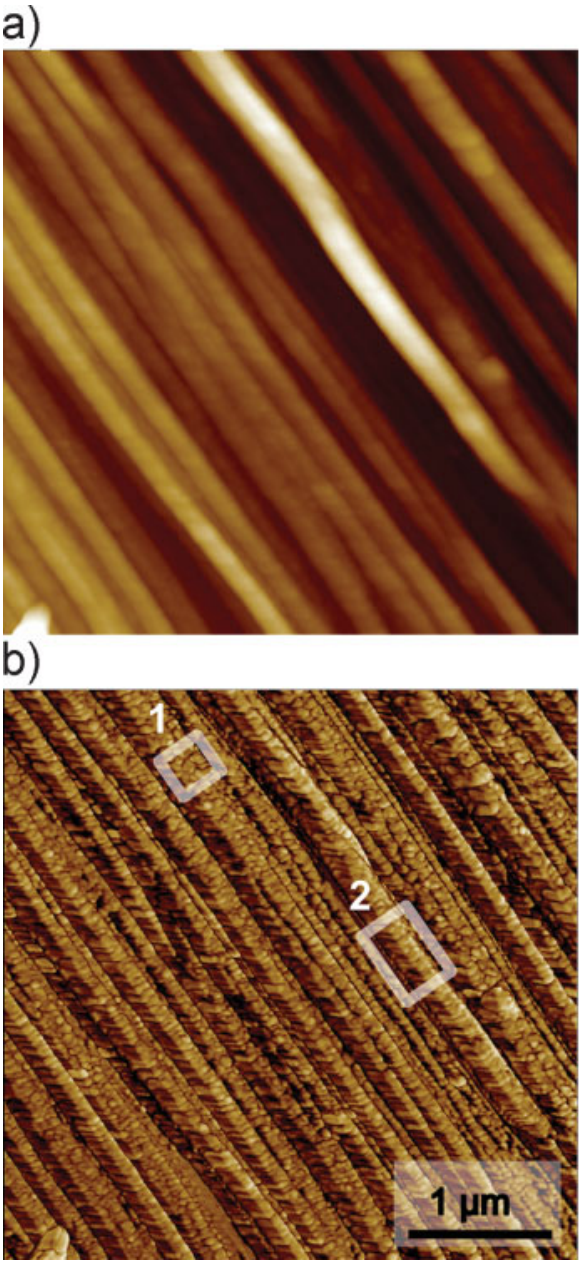

Figure 2.2. AFM images of directionally crystallized P3HT thin films: (a) height mode (b) phase mode [11].

To describe the charge transport in disordered organic materials, thermally activated hopping in a distribution of localized states is used. For instance, in variable range hopping (VRH) model charges can hop short distances with high activation energies or long distances with low activation energies. To model charge transport in well ordered conducting and semiconducting polymers the multiple trapping and release model (MTR) are used. In the MTR model it is assumed that transport occurs in bands. However, charge carriers are trapped in localized states and they can be released by thermal activation [19].

2.3. Thermal Conductivity

There are mainly three different mechanisms that cause heat transfer: radiation, convection, and conduction. Main mechanism of heat transfer is heat conduction in solid materials [20]. Heat conduction is calculated using:

$$\overrightarrow{Q} = -\lambda \overrightarrow{\nabla} T \tag{2.1}$$

where $\overrightarrow{Q}$ is heat flux, λ is thermal conductivity, and $\overrightarrow{\nabla}$T is absolute temperature gradient [21]. Thermal conductivity is the sum of different heat transferring methods.

Electron transport and phonon transport are the two main methods of heat conduction in solids. The electronic thermal conductivity is very similar to electrical conductivity [20]. The difference between the electrical conductivity and the electronic thermal conductivity is that the latter one accounts for the thermal energy instead of charge [22]. Phonons are the quanta frequency of atomic vibrations and heat energy is transferred through interactions with themselves and subatomic particles by phonons. The scattering of phonons determine the effectiveness of heat transfer as phonons propagate through the material. As a result, a different atom or a missing atom could alter the propagation of the vibration energy through the material [20].

Main heat conduction method in dielectric polymers is phonon transport. Conducting and semiconducting polymers are electrically conductive, however; their ther-

mal conductivity is essentially due to phonon transport [20].

Phonon transport dominates the heat conduction in silicon, even in the presence of large concentrations of free charge carriers. As a result, thermal conductivity of silicon decreases with the increasing numbers of charge carriers because of the lattice imperfections [23]. Conducting and semiconducting polymers may experience the same phenomenon because of their semiconductivity.

2.4. Conclusion

Conducting and semiconducting polymers conduct electricity with the mechanisms mentioned in Section 2.2. Main heat transfer mechanism in polymers is phonon transfer and thermal conductivity of the conducting and semiconducting polymers may not increase excessively compared to electrical conductivity with doping. Low thermal conductivity and high electrical conductivity make conducting and semiconducting polymers promising materials for thermal patterning.

3. THERMOELECTRIC MATERIALS

Materials that show thermoelectric effect in a convenient way are called thermoelectric materials. Thermoelectric effect defines the conversion of heat to electricity or vice versa. Basic principles underlying this process is summarized in this chapter.

3.1. Seebeck Effect

The schematic of a basic thermocouple is shown in Figure 3.1 to discuss the thermoelectric energy. Two dissimilar conductors, which are called thermoelements, are connected electrically series and thermally in parallel. When the temperatures of the junctions T_A and T_B are different an open circuit elctromotive force (emf), V is developed between C and D. The emf is given by:

$$V = \alpha \left| T_A - T_B \right| \tag{3.1}$$

and the differential Seebeck coefficient α_{ab} is given by:

$$\alpha = V/\Delta T \tag{3.2}$$

Moreover, for small temperature differences the relationship is linear and Seebeck coefficient is constant for a given temperature [24].

3.2. Thermoelectric Generation and the Figure-of-Merit

As a heat engine thermoelectric heaters obey the laws of thermodynamics. The efficiency is defined as the ratio of the electrical power delivered to the load to the heat

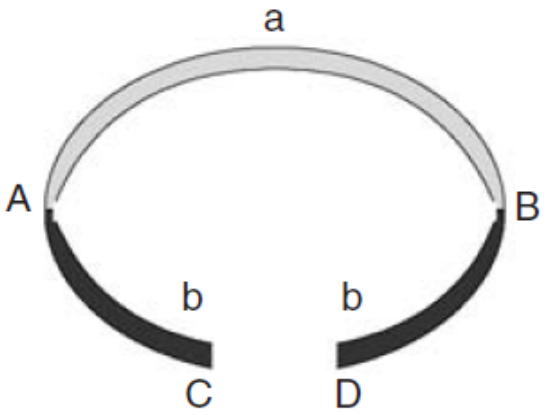

Figure 3.1. Schematic of a basic thermocouple [24].

absorbed at the hot junction. Therefore, the efficiency of the generator is given by [24]:

$$\phi = \frac{energy\ supplied\ to\ the\ load}{energy\ absorbed\ at\ hot\ junction} \tag{3.3}$$

The electrical conductivities, thermal conductivities, and Seebeck coefficients are assumed to be constant within an arm. Contact resistances are assumed to be 0 because they are negligible compared to sum of the arm resistances [24].

$$\phi = \frac{I^2 R}{\alpha_{ab} T_H = \lambda' \left(T_H - T_C\right) - \frac{1}{2} I^2 R} \tag{3.4}$$

where λ' is the thermal conductance of a and b in parallel and and R is the electrical resistance of a and b in series. To acquire a acceptable result average values of α, λ',and σ are adopted because these values change with temperature [24].

Efficiency is a function of the ratio of the load resistance to the sum of the generator arm resistance and the efficiency at the maximum power can be shown as [24]:

$$\phi_p = \frac{T_H - T_C}{\frac{3T_H}{2} + \frac{T_C}{2} + \frac{4}{Z_C}} \tag{3.5}$$

while

$$\phi_{max} = \eta_c \gamma \tag{3.6}$$

where

$$\eta_c = \frac{T_H - T_C}{T_H} \tag{3.7}$$

$$\gamma = \frac{\sqrt{1 + Z_C \bar{T}} - 1}{\sqrt{1 + Z_C \bar{T}} + \frac{T_C}{T_H}} \tag{3.8}$$

$$\bar{T} = \frac{T_H + T_C}{2} \tag{3.9}$$

$$Z_C = \frac{{\alpha_{ab}}^2}{R\lambda'} \tag{3.10}$$

If it is assumed that geometries of a and b are matched and the two arms of the junction have similar material constants:

$$Z = \frac{\alpha^2 \sigma}{\lambda} \tag{3.11}$$

where $\alpha^2\sigma$ is the electrical power factor [24].

The figure of merit derived assuming that thermal conductivity, electrical conductivity and Seebeck coefficient are independent of temperature. Moreover, to increase available heat conversion temperature can be increased [24]. As a result, the figure of

merit can be advanced to:

$$ZT = \frac{\alpha^2 \sigma}{\lambda} T \tag{3.12}$$

3.3. Thermoelectric Materials

In terms of electrical conductivity, metals are much more conductive compared to insulators. In addition to this semiconductors occupies an intermediate position between metals and insulators. Electrical conductivity is a reflection of charge carrier concentration like thermal conductivity and Seebeck coefficient. With the increasing charge carrier concentration electrical conductivity and thermal conductivity increases wheras Seebeck coefficient decreases as shown in Figure 3.2 [24].

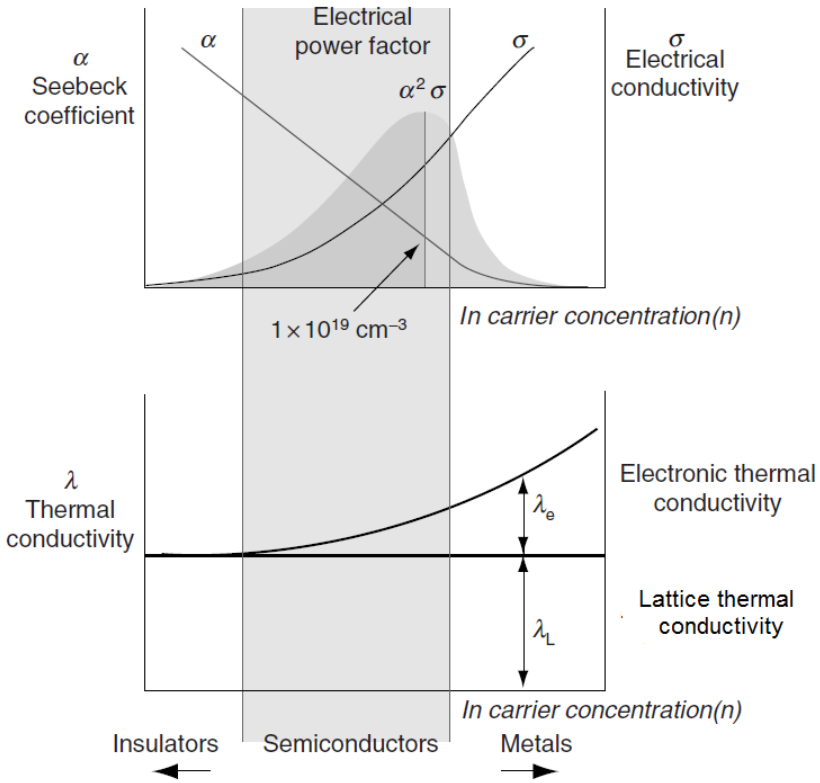

Figure 3.2. Carrier concentrations vs electrical conductivity, thermal conductivity, Seebeck coefficient and power factor [24].

Almost all conducting materials (except for superconductors) exhibits thermoelectric phenomena. Materials which posesses a ZT>0.5 are usually regarded as thermoelectric materials [24]. Inorganic thermoelectric semiconductor materials such as Bi_2Te_3, PbTe, BiSb, $CoSb_3$, SiGe, and MgSi has been focused on to have high ZT values. A ZT value of 2.4 can be realized with these materials [25].

3.4. Conclusion

To obtain a high thermoelectric figure of merit low thermal and high electrical conductivity is necessary and conducting and semiconducting polymers are candidates for thermoelectric applications. Early reports on conducting and semiconducting polymers indicated that stable ZT values of on the order of 10^{-2} - 10^{-3} can be achieved [25]. Later studies show that higher ZT values can be reached. Kong *et al.* showed that composite films obtained from a PEDOT:PSS aqueous solution by simultaneous addition of dimethyl sulfoxide (DMSO) and different concentrations of urea a ZT value of 0.024 can be reached [26]. To increase the thermoelectric performance PEDOT:PSS/Bi_2Te_3 composite films are formed by Song and co workers and a ZT value of 0.04 is obtained [27]. PEDOT:PSS/Bi_2Te_3 composites are also studied by Zhang *et al.* and they have achieved to obtain a ZT value of 0.08 [28]. A study shows that a ZT value of 0.25 can be achieved by controlling the oxidation level of PEDOT [3]. Despite the fact that ZT value of conducting and semiconducting polymers are lower compared to inorganic thermoelectric materials, compared to inorganic materials conducting and semiconducting polymers have advantages like low cost due to abundance of carbon resources, easy synthesis, abundant electron energy bands through modulating, easy processing into versatile forms, high energy density, and low thermal conductivity. Moreover, conducting and semiconducting polymers are promising candidates for high efficiency thermoelectric materials because of the unique and various electronic band structures [25].

4. THERMOELECTRICAL PROPERTIES OF P3HT

To analyze the usability of P3HT in thermoelectric applications and thermoelectric patterning thermoelectrical properties of P3HT is analyzed and an experimental setup to measure the lateral thermal conductivity is described in this chapter.

4.1. Thermal Conductivity

Thermal coefficients of bulk materials and thin films can be different and most of the thermal conductivity measurement techniques are useful for bulk samples. As mentioned in Section 2.1 physical properties of the conducting and semiconducting thin film polymers are anisotropic. As a result, material properties should be measured in the same form as the one used in the application. Thermal conductivity measurement techniques can be grouped as [29]:

- Pulse Techniques
- Steady State Techniques

4.1.1. Pulse Techniques

There are numerous methods that uses pulse techniques for thermal conductivity measurements. For instance, in thermo reflectance technique, the temperature change caused by a laser beam is sensed by another laser beam. However, density and specific heat of the materials, which are often not known exactly for a polymer material, must be known in these methods [29].

In other non steady state techniques, microelectrode structures are used as heat source and temperature sensor [29] and small third harmonic voltage component is used while applying an alternating current through the heat source. Both thermal conductivity and specific heat can be measured with this method which is called 3-omega technique [30]. Approximate solutions were obtained for low frequencies in

order to measure thermal conductivity [31]. However, much simpler formula exists for high frequencies [32].

4.1.1.1. 3-omega Technique. In 3-ω technique a micro fabricated metal strip is deposited on the thin film surface which acts as a heater and thermometer which is shown in Figure 4.1. An alternating current with ω frequency is passed through the metal strip which causes heat at the second harmonic. Because the electrical resistance of the strip, which is influenced by the temperature, changes with the time by measuring 3-ω voltage across the strip temperature oscillations can be measured indirectly [33].

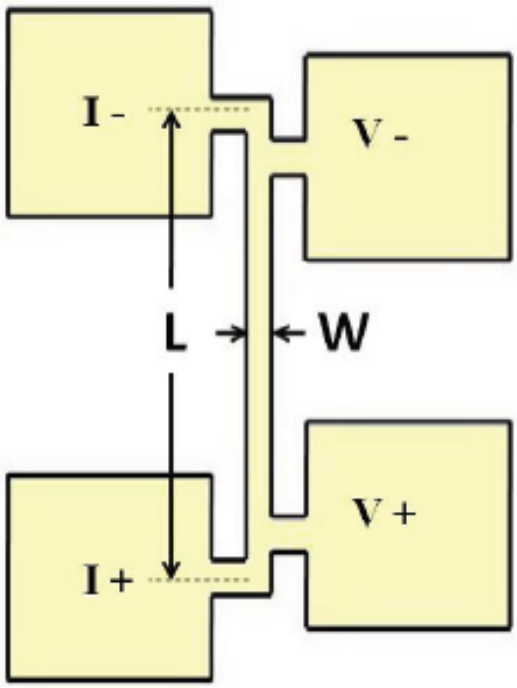

Figure 4.1. Schematic of the heater strip [33].

The outer pads which can be seen in Figure 4.1 are used for connecting probes and the inner ones measure the electrical potential of the heater. An alternating current is passed through the heater:

$$I_0(t) = I_0 cos(\omega t) \tag{4.1}$$

where I_0 is peak current amplitude and $I_0(t)$ is the instantaneous current. The alternating current generates a heat which can be shown as:

$$P_0(t) = \frac{1}{2} I_0^2 R_0 (1 + cos(2\omega t)) \tag{4.2}$$

where P_0 is the instantaneous power produced by the heater strip and the R_0 is the nominal resistance. This power causes temperature difference which can be separated as direct and alternate components as follows:

$$\Delta T = \Delta T_{DC} + |\Delta T_{AC}| \, cos(2\omega t + \varphi) \tag{4.3}$$

where φ is the phase shift. The heat stays in the heater if the thermal conductivity of the substrate is low which causes large temperature oscillations. Resistance of the heater is used to measure the temperature variation over time.

$$R(t) = R_0(1 + \beta \Delta T_{DC} + \beta \, |\Delta T_{AC}| \, cos(2\omega t + \varphi)) \tag{4.4}$$

where β is the temperature coefficient of resistance of the heater. Combining Equation 4.2 and Equation 4.4 results as:

$$V(t) = I_0 R_0 \left[(1 + \beta \Delta T_{DC}) cos(\omega t) + \frac{1}{2} \beta \, |\Delta T_{AC}| \, cos(\omega t) + \frac{1}{2} \beta \, |\Delta T_{AC}| \, cos(3\omega t) \right] \tag{4.5}$$

In Equation 4.5 last voltage component has 3ω frequency which is 1000 times smaller than the first harmonic voltage [34] and contains useful information about thermal conductivity [33].

If current passes through the heater heat conduction occurs through the sample.

$$P(t) = -\lambda \pi r l \frac{dT_{AC}(r)}{dr} \tag{4.6}$$

where λ is thermal conductivity, r is the radius, and l is the length of the heat flow profile. By integrating Equation 4.6 a general formula for radial temperature gradient caused by a 1D heater line can be inferred.

$$P \int_{r_1}^{r_2} \frac{dr}{r} = -\lambda \pi l \int_{T_1}^{T_2} dT_{AC}(r) \tag{4.7}$$

$$\Delta T_{AC}(r) = -\frac{P}{\lambda \pi l} ln \frac{r_2}{r_1} \tag{4.8}$$

By combining the third harmonic voltage component of Equation 4.5 and Equation 4.8 a general formula for thermal conductivity can be obtained.

$$\lambda = \frac{V_0^3 ln \frac{f_2}{f_1}}{4\pi l R_0^2 (V_{3\omega,1} - V_{3\omega,2})} \frac{dR}{dT} \tag{4.9}$$

where dR/dT is the rate of resistance change of the heater with its temperature variation and $V_{3\omega,1}$ and $V_{3\omega,2}$ are the third harmonic voltage at input current of f_1 and f_2 [33].

3-ω technique has some unique advantages. First of all this method has the lowest possible errors caused by blackbody infrared radiation because of micro structures of the heater and the temperature sensors. Secondly, measurements can be carried out much faster [33].

4.1.2. Steady-State Techniques

In steady state techniques, a heat flow is established through the sample. The thermal resistance is measured from the temperature difference. To calculate thermal conductivity from the thermal resistance a simple geometry should be used. Heat leakages contact resistances must be taken into account to obtain a sustainable result [29].

The duality between electrical domain and thermal domain can be used to simplify calculations in steady state techniques. With the knowledge of electrical domain, understanding thermal domain becomes easier. The duality can be summarized as shown in the Figure 4.2 [35].

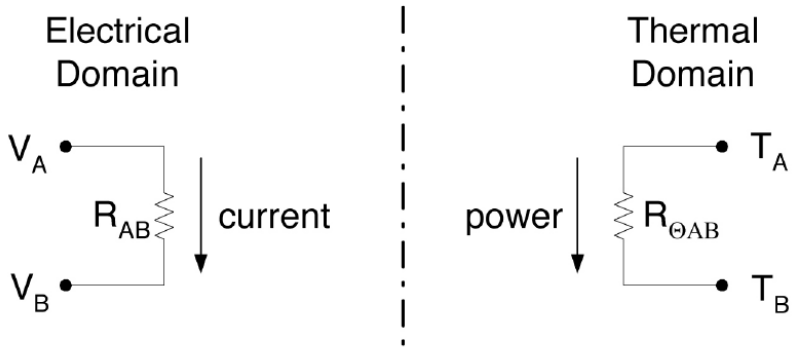

Figure 4.2. Thermal domain electrical domain duality [35].

In Table 4.1 through and across variables of the each domain are listed. The parameter that flows from one reference point to another is called the through variable. The across variable is the variable that forces the flow of the through variable. Moreover, both of the domains have a resistance that impedes the flow of the through variable [35].

4.1.2.1. Methodology of Steady State Thermal Conductivity Measurement. The advantage of the used method is that advanced measurement equipments are not needed to measure the thermal conductivity of the thin film. A special sequence of measurements are done to separate the thermal conductivity of thin polymer film material from the the leaking heat flow. Instead of taking the temperature difference between two probes, the temperature difference at one of the probe for different input power values are taken while the temperature of the other probe is kept constant [29]. A basic schematic of the method is shown in Figure 4.3.

Table 4.1. Basic relationships in electrical and thermal domains [35].

	Electrical Domain			Thermal Domain		
	Variable	Symbol	Units	Variable	Symbol	Units
Through Variable	Current	I	Amperes or Coulombs/s	Power or Heat Flux	Q	Watts or Joules/s
Across Variable	Voltage	V	Volts	Temperature	T	C or K
Resistance	Electrical Resistance	R	Ohms	Thermal Resistance	W	°C/W or K/W
Capacitance	Electrical Capacitance	C	Farads or Coulombs/V	Thermal Capacitance	C_T	Joules / °C
"Ohm's Law"	δV = I R			δT = Q W (derived from Fourier's Law) (derived from Fourier's Law)		

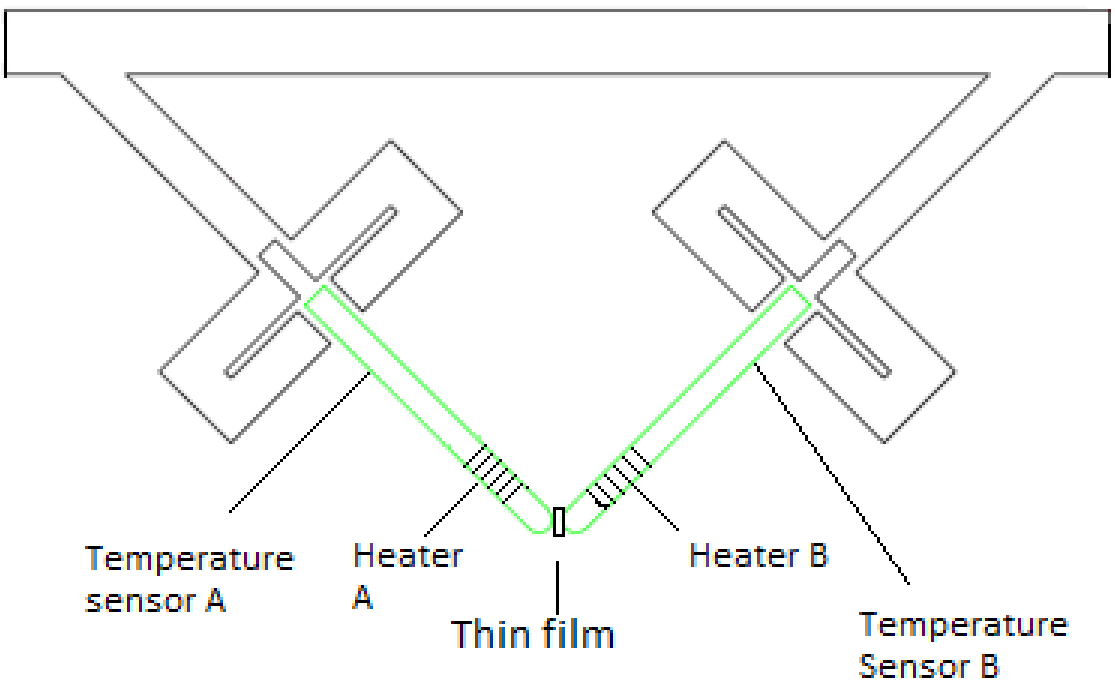

Figure 4.3. Schematic of the system.

To obtain a heat flow from probe A to probe B through the film sample probe B is not powered in the first step. The power supplied to the system is equal to [29]

$$P = \frac{T_B^{(0)} - T_A}{W_{tot}} = \frac{T_{out} - T_A}{W_{tot} + W_{leak}} \tag{4.10}$$

where the subscript (0) indicates without heating. In the second step the probe B is also heated. As a result, the created heat power P_{in} flows form the heater to base and to the environment [29].

$$P_{in} = P_B + P_A = \frac{T_B - T_A}{W_{tot}} + \frac{T_B - T_{out}}{W_{leak}} \tag{4.11}$$

Solving Equation 4.10 for T_{out} and inserting into Equation 4.11:

$$P_{in} = \frac{W_{leak} + W_{tot}}{W_{leak} \mathrm{x} W_{tot}} \mathrm{x} \left(T_B - T_B^{(0)} \right) \tag{4.12}$$

Assuming that leaking heat resistance is much larger than the thermal resistance between the base and the heater the Equation 4.12 simplifies to [29]:

$$W_{tot} = \frac{T_B - T_B^{(0)}}{P_{in}} \tag{4.13}$$

If $W_{leak} >> W_{sample}$ is achieved, leakage of heat to the environment is negligible and the thermal resistance of the sample is measured using the temperature difference of probe B with and without heating.

When the thermal resistance of the thin film material is measured, the thermal conductivity of the material can be calculated easily if it has a simple geometry with

the formula which is derived from Fourier's Law for heat conduction [21].

$$W = \frac{L}{\lambda A} \tag{4.14}$$

where L is length and A is area.

4.1.3. Experimental Setup of Thermal Conductivity Measurement

Materials and equipments that are used in the thermal conductivity measurement are listed below:

- Acrylic glass material
- Omega RTD-800 PT100 temperature sensor
- Agilent 34410A multimeter
- Insulated copper wires
- Nanovak vacuum chamber
- Hameg triple power supply HM7042-5

Acrylic glass Poly(methyl methacrylate) material is used as a holder material for RTD-800 temperature sensors. Acrylic glass is used because it is easy to shape and it has a relatively low thermal conductivity (thermal conductivity of acrylic glass is 0.2 $\mathrm{Wm}^{-1}K^{-1}$.). Dimensions of the acrylic glass holder is shown in Figure 4.4.

Insulated coper wires are used as heaters and they are tightly coiled up around the RTD-800 PT100 temperature sensors; which is shown in Figure 4.5. Thin wires are used to increase the resistance and decrease the current. Hameg triple power supply HM7042-5 power supply is used to heat up the system. It has 0.01 V voltage sensitivity and can swing between 0- 32 V and 0-2 A. Sensitivity of the DC voltage supply is important to adjust the temperature to the wanted value.

34410A digital multimeter with $6\frac{1}{2}$ digit enhanced performance is used to measure the resistance of the PT100 temperature sensor. To increase the sensitivity of the

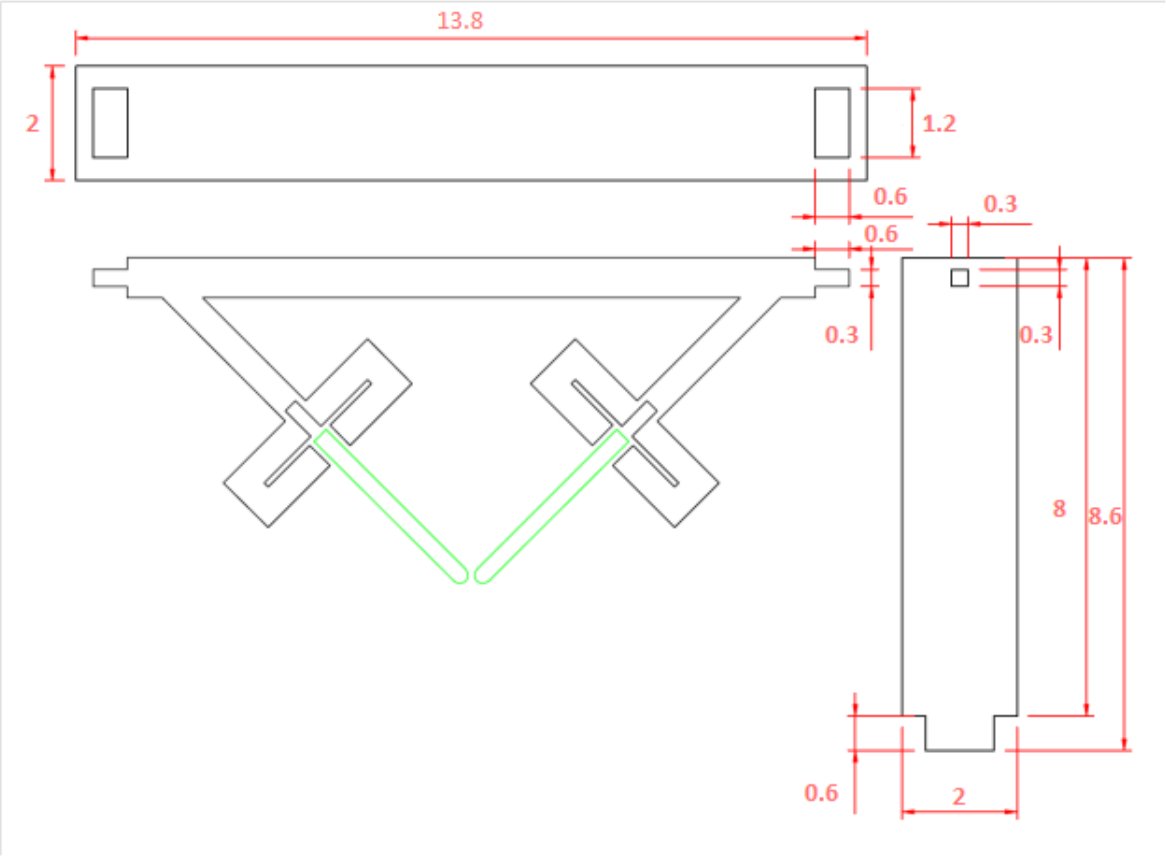

Figure 4.4. Dimensions of the holder. (Lengths are in cm.)

Figure 4.5. Omega RTD800 PT100 temperature sensor.

temperature sensor a high digit multimeter should be used.

Vacuum chamber is used because heat leakage is reduced in vacuum environment. To increase the leakage resistance which causes measuring the thermal resistance of the sample more accurately the experiments are done in a vacuum chamber.

In Figure 4.6 the acrylic glass holder, temperature sensors and the heating coils are shown and in Figure 4.7 vacuum chamber multimeter and DC power supply are shown.

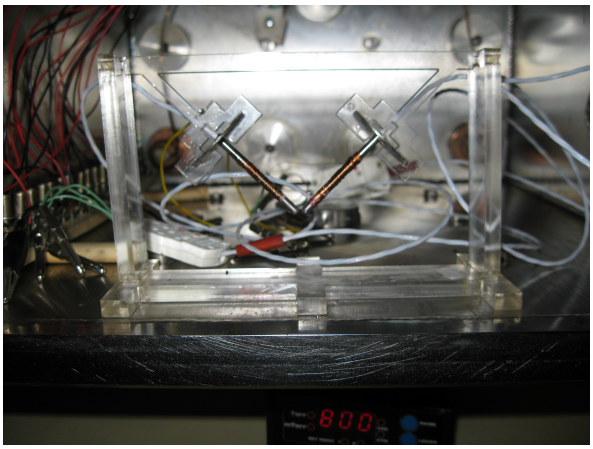

Figure 4.6. Holder, temperature sensors, and the heater coils.

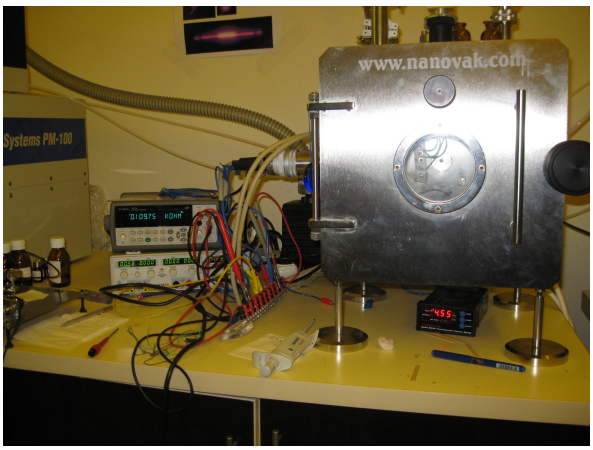

Figure 4.7. Vacuum chamber, multimeter,and dc power supply.

The established experimental setup measures the lateral thermal conductivity of the method explained in Section 4.1.2.1. One of the RTD-800 temperature sensor and copper coil is employed as probe A and the other one is employed as probe B. The sample to be measured is placed between the temperature sensors and the thermal resistance of the sample is measured using the Equation 4.13.

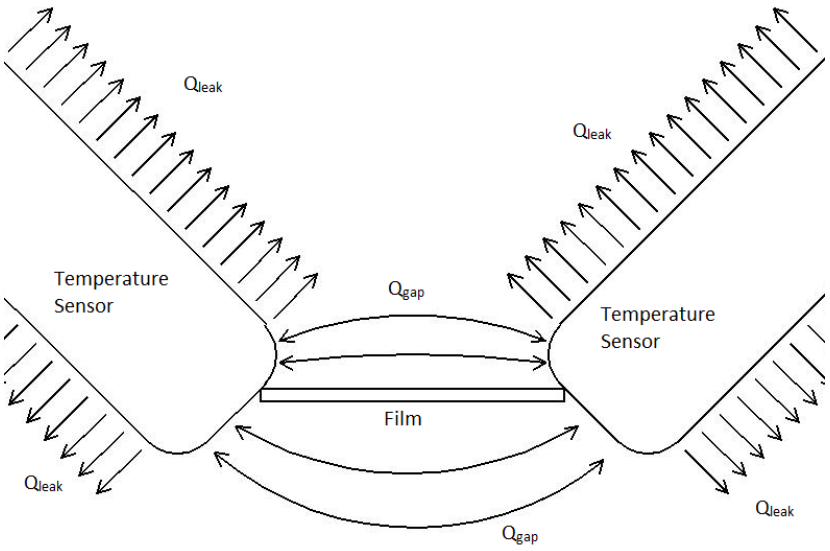

Figure 4.8. Vacuum chamber, multimeter,and dc power supply.

Figure 4.8 shows the heat leakages from the temperature sensors. To have opinion about the precision of the experimental setup Knudsen number (Kn) of the vacuum ambient should be calculated using:

$$Kn = \frac{mean\ free\ path}{L} \tag{4.15}$$

where L is the length characteristic of the flow. Mean free path of air can be calculated with [36]:

$$mean\ free\ path = \frac{(2.08\text{x}10^{-7})T^2}{(T + 198.6)p} \tag{4.16}$$

where mean free path is in inches, T is temperature in °R, and p is pressure in inches of mercury. After necessary conversions the mean free path of air at 50 °C at 2 Torr is calculated and is equal to 2.9x10^{-5}m. Kn for the gap between the probes is approximately 0.0209. Because the Kn is less than 0.1 radiative, convective, and conductive heat transfer should be taken into account. To simplify the calculations only the radiative and conduction heat transfers between the temperature sensors are calculated and the gap is modeled as two parallel square surfaces [36]. View factor (F) of aligned parallel squares can be calculated using:

$$F = \frac{2}{\pi \overline{X}^2}\left\{ ln\left[\frac{(1+\overline{X})^2}{1+2\overline{X}^2}\right]^{1/2} + 2\overline{X}(1+\overline{X}^2)^{1/2} tan^{-1}\frac{\overline{X}}{(1+\overline{X}^2)^{1/2}} - 2\overline{X} tan^{-1}\overline{X}\right\} \quad (4.17)$$

where X is the edge length of the square, L is the length of the gap, and the $\overline{X}$ is X/L [37]. For X=3mm and L=1mm F is equal to 0.547. Radiative heat transfer is calculated using the circuit in Figure 4.9. A is area of the square, σ is the Stefan-Boltzman constant, E_i is σT^4, and ε is emissivity. ε of stainless steel is 0.21 [37]. The temperature of probe A is around 60 °C and the temperature of the probe B is around 45 °C when it is not heated. For the given values radiative heat transfer is equal to 8.66 mW. Thermal conductivity of air at 2 Torr is equal to 7.2x10^{-3} Wm^{-1}C^{-1} and heat transfer by conduction is equal to 97.2mW [36]. The thermal resistance between the probes caused by radiation and conduction is equal to 142 K/W. However, this calculation may not be correct because of the assumptions.

Heat leakage from temperature sensors is calculated because of the $W_{leak} >> W_{sample}$ assumption. The calculations are done with the assumptions room temperature is 25 °C and the temperature of the tip of the sensor is 50 °C. One of the leakage source is the heat conduction of the sensor itself an it is calculated using:

$$Q = \lambda A \Delta T \quad (4.18)$$

where A is area, λ is thermal conductivity and ΔT is the temperature difference. Thermal conductivity of stainless steel is taken from Table 1.1. Leakage heat from the conduction is equal to 9x10^{-4} W. Radiative heat loss from the sensor is also calculated

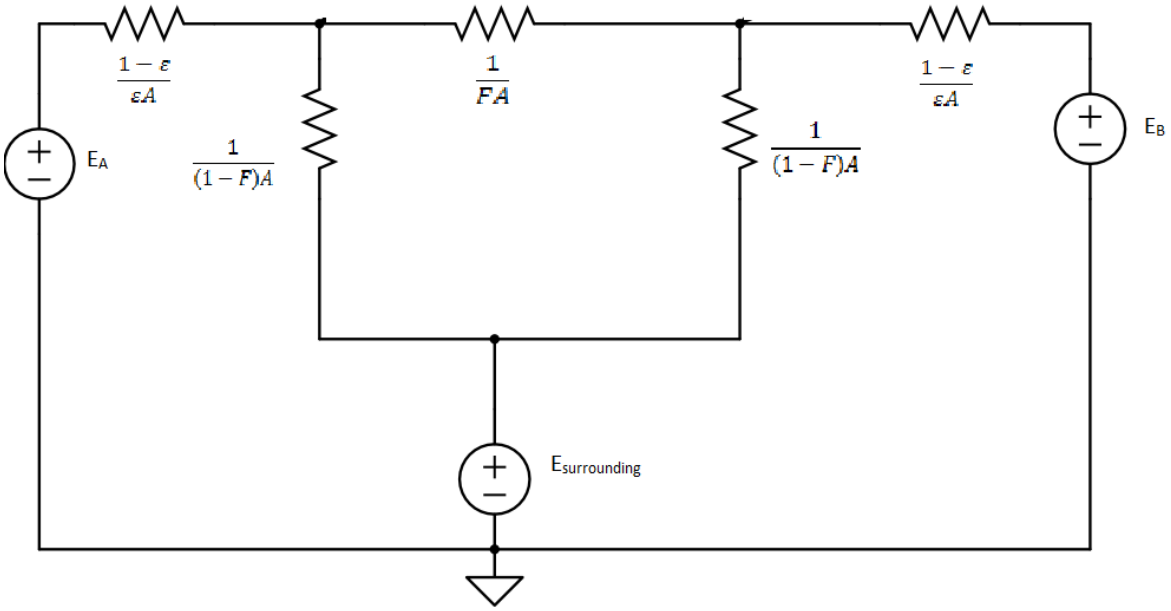

Figure 4.9. Schematic of radiative heat conduction of the gap.

using the equation:

$$Q = \varepsilon\sigma 2\pi r \int_0^L (T_S^4(x) - T_{out}^4)dx \tag{4.19}$$

where ε is the emissivity, A is the surface area, σ is the Stefan-Boltzman constant, L is the length of the sensor, T_S is the temperature of the surface, and T_{out} is the chamber temperature. Radiative heat loss is approximately equal to $2\text{x}10^{-4}$W. Total heat leakage is $1.1\text{x}10^{-3}$ W. Leakage resistance is $2.27\text{x}10^4$ K/W.

In addition to leakage, tolerance of the temperature sensors may be a main source of measurement error. The tolerance of the sensors changes with the temperature and as seen in the Figure 4.10 and can be calculated using the formula [38]:

$$\Delta^\circ C = \pm(0.15 + 0.002T) \tag{4.20}$$

where T is temperature in °C. The tolerance of the multimeter is ignored because it is negligible compared to the tolerance of the temperature sensor which is equal to ±0.009°C.

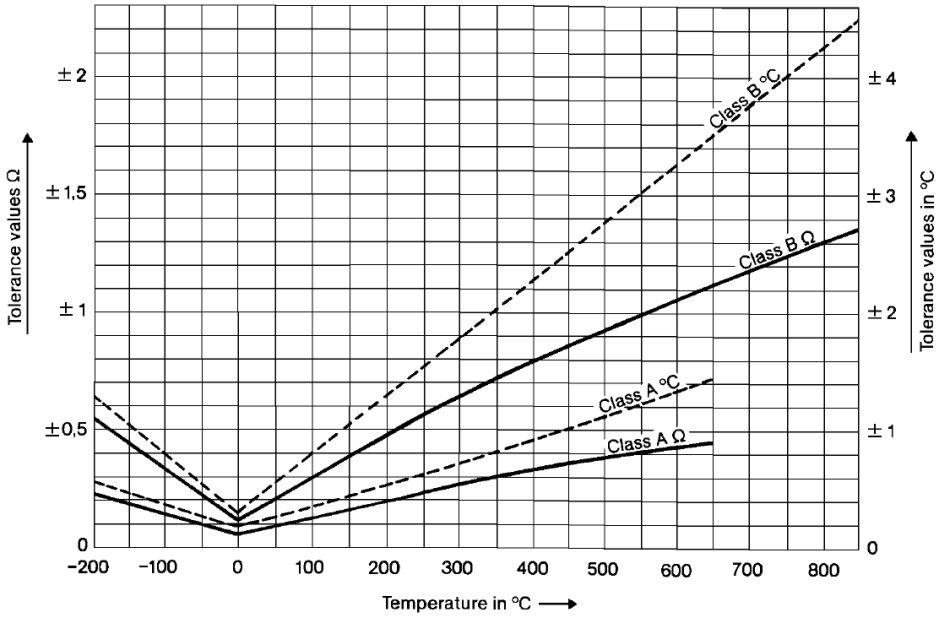

Figure 4.10. Tolerance of platinum sensors vs temperature graph [38].

4.1.4. Thermal Conductivity Measurement Results

4.1.4.1. Thermal Resistance of the Gap. In order to measure the thermal conductivity of the semiconducting polymer thin film thermal conductivity of the gap between two temperature sensors, which is a parallel thermal resistance to the thermal resistance of the semiconducting polymer film, is measured. To measure the thermal resistance of the gap no film was formed between the thermal probes. The measured values are taken after they stabilize, which takes usually more than 3 hours. To be sure that resistance values are stabilized resistance change over time is observed via LabVIEW. The measurements are done in a vacuum environment which has a pressure between 1-2 Torr to reduce the heat transfer by the heat conduction of air and convection of air. More than 30 measurements are done to obtain a constant T_A for different P_B values. Only successful measurements are shown in Table 4.2 where I is input current, V is input potential difference, P is input power, ΔR is resistance change in temperature

sensor and subscripts A and B defines probe A and probe B.

Table 4.2. Measurement results to calculate thermal resistance of the gap.

I_A (A)	V_A (V)	I_B (A)	V_B (V)	P_A (W)	P_B (W)	ΔR_A(Ohm)	ΔR_B (Ohm)
0.080	1.50	0	0	0.1200	0	5.74	0.88
0.072	1.45	0.127	0.40	0.1131	0.0508	5.72	2.31
0.071	1.43	0.157	0.50	0.1015	0.0785	5.75	3.10
0.069	1.40	0.188	0.60	0.0966	0.1128	5.72	4.02

Temperature of the base sensor is calculated from the resistance values. To obtain temperature values β (temperature coefficient of resistance) of PT-100, which is equal to 0.00385 ohm/ohm/°C, is used in Equation 4.21.

$$R = R_0 \left[1 + \beta \left(T - T_0\right)\right] \tag{4.21}$$

Power versus T_B graph, which is shown in Figure 4.11 can be drawn with the measured power and calculated temperature.

Thermal resistance of the gap is calculated from the slope of the graph in Figure 4.11. Because of the change in the temperature of the system, the tolerance of the temperature sensor changes causes ±0.16 uncertainty, which is calculated using Equation 4.20.

$$W_{gap} = 74.43 \pm 0.16 ^{\circ}C/W \tag{4.22}$$

4.1.4.2. Thermal Resistance and the Thermal Conductivity of Polyimide Film. Thermal resistance of a thin film with a known thermal conductivity should be measured to verify the experimental setup. Thermal resistance of GoodFellow Kapton HN film with

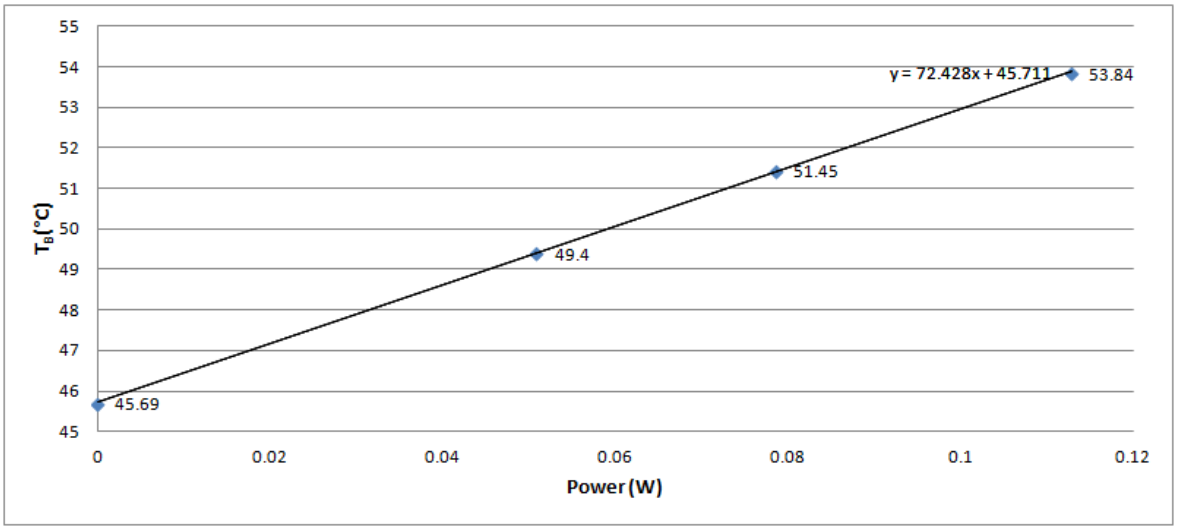

Figure 4.11. Power versus T_B graph of the system with no film.

125±14 μm thickness is measured. The width and the length of the film is measured Nikon measuring microscope MM-400 shown in Figure 4.12. The width of the film is 5.55 mm and the length of the film is 1.01 mm. In order to reduce the contact resistance between the polyimide film and the temperature sensor Omegatherm 201 high temperature high thermal conductivity paste is used. After these preliminary preparations same steps are followed that are done in measurement of thermal resistance of the gap.

More than 20 measurements are done to obtain a constant T_B for different P_B values. Only successful measurements are shown in Table 4.3.

After the measured resistance values are converted to temperature values using Equation 4.21 the power vs temperature graph is drawn as shown in Figure 4.13.

As seen from the graph thermal resistance of the system is equal to:

$$W_{Polyimide//gap} = 72.52 \pm 0.16°C/W \tag{4.23}$$

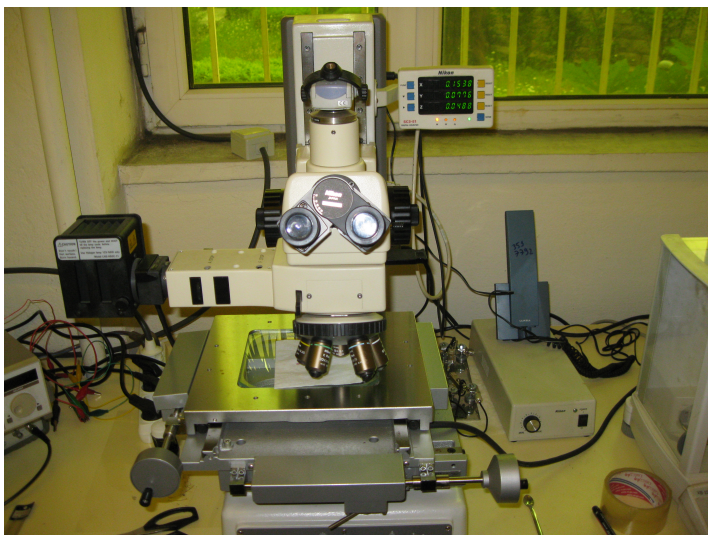

Figure 4.12. Nikon measuring microscope MM-400.

Table 4.3. Measurement results to calculate thermal resistance of the polyimide film.

I_A (A)	V_A (V)	I_B (A)	V_B (V)	P_A (W)	P_B (W)	ΔR_A(Ohm)	ΔR_B (Ohm)
0.075	1.50	0	0	0.1125	0	5.74	0.90
0.072	1.44	0.127	0.40	0.1037	0.0508	5.72	2.32
0.070	1.42	0.157	0.50	0.0994	0.0785	5.74	3.10
0.068	1.39	0.188	0.60	0.0945	0.1128	5.73	4.06

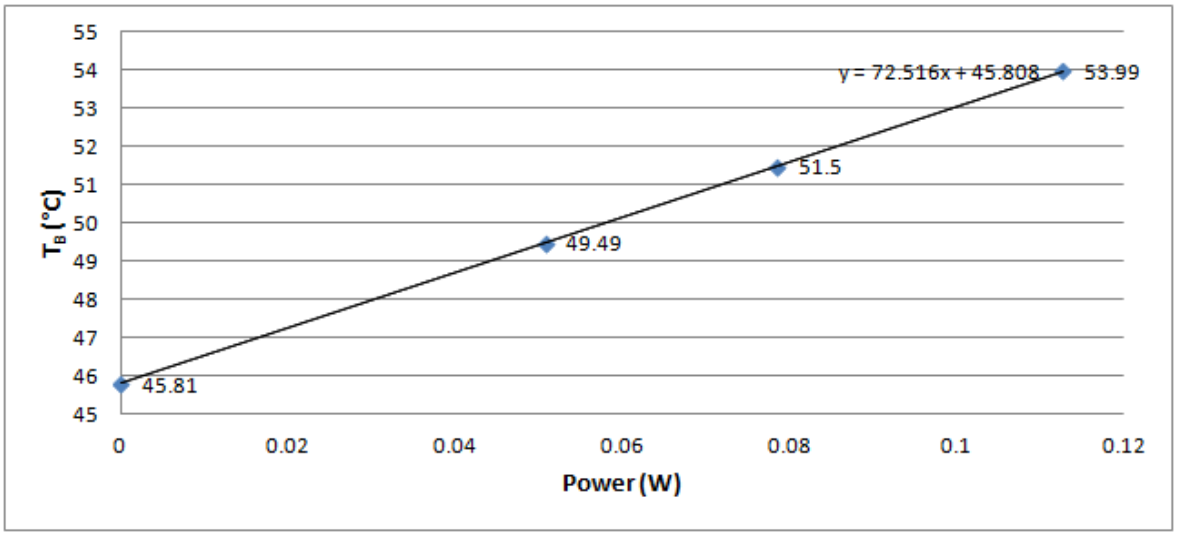

Figure 4.13. Power versus T_B graph of the system with polyimide film.

Thermal resistance of the polyimide film is calculated from the total resistance:

$$72.52 = \frac{W_{Polyimide}\text{x}74.43}{W_{Polyimide} + 74.43} \tag{4.24}$$

$$W_{Polyimide} = 2826 \pm 572^{\circ}C/W \tag{4.25}$$

To calculate thermal conductivity from the thermal resistance equation 4.14 is used and tolerances of the temperature resistances and film thickness are included:

$$2826 = \frac{1.01\text{x}10^{-3}}{\lambda_{polyimide}\text{x}125\text{x}10^{-6}\text{x}5.5\text{x}10^{-3}} \tag{4.26}$$

$$\lambda_{polyimide} = 0.516 \pm 0.127 W m^{-1} C^{-1} \tag{4.27}$$

The thermal conductivity of the polyimide film is 0.35 W m^{-1} $°C^{-1}$ at room temperature as indicated in the website of the producer. It is assumed that the thermal conductivity of the polyimide does not change with temperature. The error of the measurement is calculated below for the given film:

$$\%error = \frac{0.516 - 0.35}{0.35} \text{x} 100 = 47.43\% \tag{4.28}$$

The high error of the measurement have different causes. It is obvious that $W_{polyimide} >> W_{gap}$ and this kills the sensitivity of the measurement. To increase the W_{gap} surface area of the gap should be decreased. In addition pressure of the environment can be decreased. Moreover, leakage resistance and the tolerances of the temperature sensors add error to the measurement.

To reduce the effect of contact resistances in the measurement of the resistance of the temperature sensor, 3 wire construction is used. As shown in Figure 4.14 the third wire remove the average lead wire resistance from the measurement. Even so; small errors may still occur in the measurement.

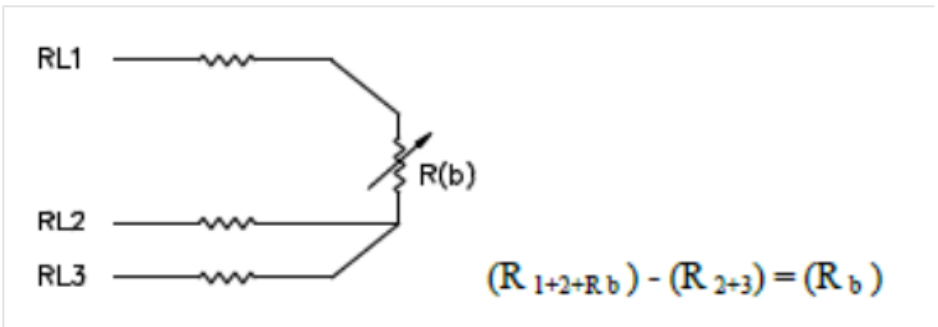

Figure 4.14. 3-wire construction.

As mentioned above there are different sources that increases the error of the measurement. However, the measurement still can determine the order of magnitude of the thermal conductivity of the material with a cheap experimental setup.

4.1.4.3. Thermal conductivity of the Poly (3-hexylythiophene). Polymeric semiconductor that is used in the measurement is prepared from P3HT (Poly (3-hexylythiophene)) (95% regioregular) purchased from Sigma-Aldrich Co. The polymer is dissolved in chloroform for 2 hours at 40 °C resulting to concentration of 2mg/ml. To form the film between the temperature sensors the following method is used. A small container is placed under the temperature sensors and filled with DI water as shown in Figure 4.15. After that the P3HT is carefully dropped on the DI water between the temperature sensors with drop casting method. After the chloroform and some of the DI water evaporated the container is taken away from the environment and the film is formed between the temperature sensors as shown in Figure 4.16.

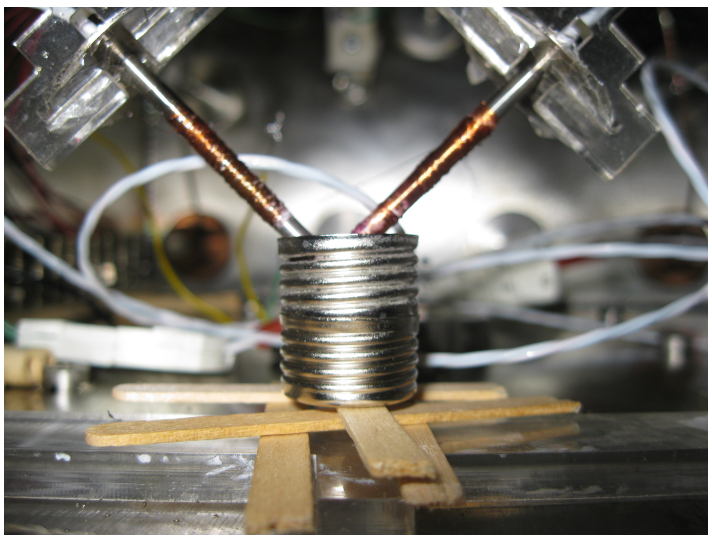

Figure 4.15. Container that is used to form the film between the temperature sensors.

After the film is formed, the same steps that are done for measuring the thermal conductivity of the gap and the polyimide film is repeated.

As seen from the graph thermal resistance of the system:

$$W_{P3HT//gap} = 74.39 \pm 0.16°C/W \tag{4.29}$$

Because the tolerance of the system is greater than the difference between W_{gap} and $W_{P3HT//gap}$, the tolerance of the experimental setup is ignored. If the thermal resistance

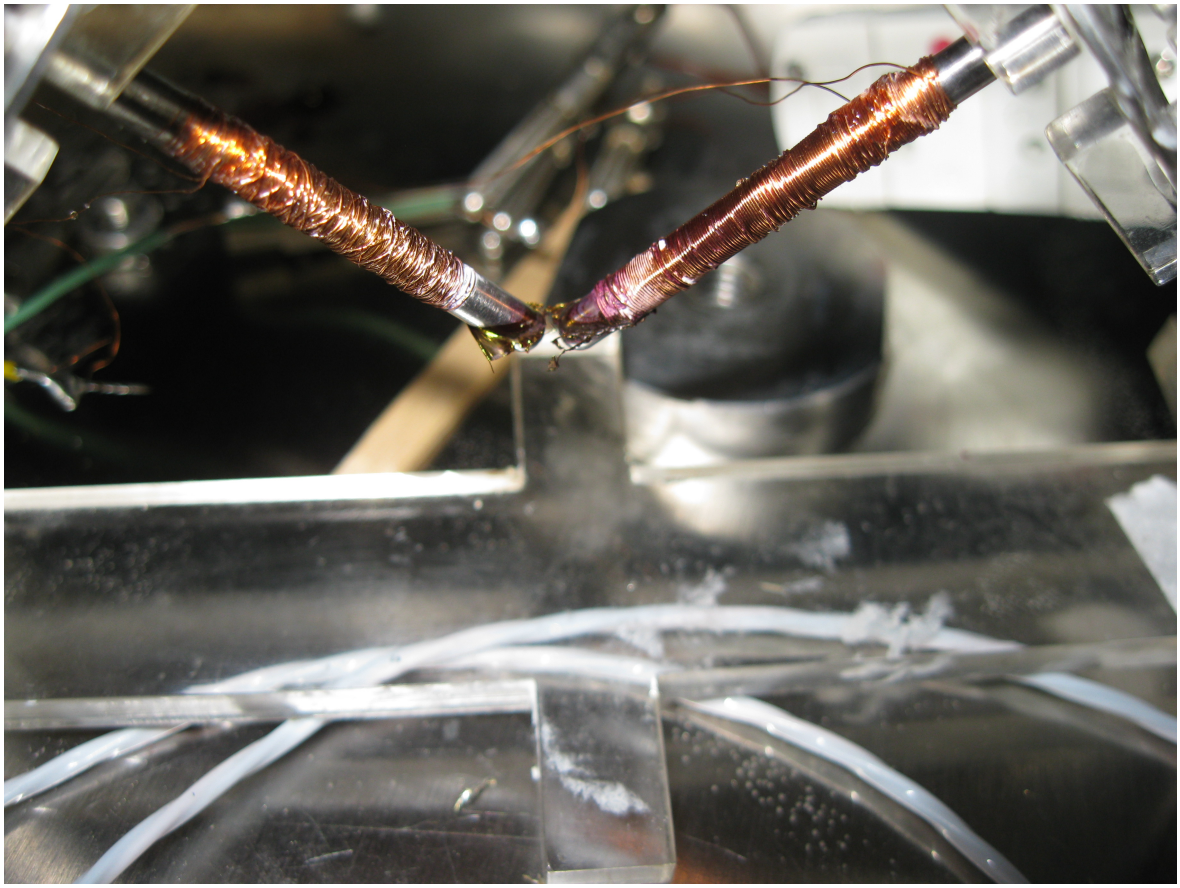

Figure 4.16. P3HT film formed between the temperature sensors.

Table 4.4. Measurement results to calculate thermal resistance of the P3HT film.

I_A (A)	V_A (V)	I_B (A)	V_B (V)	P_A (W)	P_B (W)	ΔR_A(Ohm)	ΔR_B (Ohm)
0.075	1.50	0	0	0.1125	0	5.75	0.88
0.072	1.45	0.126	0.40	0.1131	0.0504	5.74	2.31
0.071	1.42	0.156	0.50	0.1008	0.0780	5.73	3.12
0.069	1.39	0.186	0.60	0.0959	0.1116	5.72	4.07

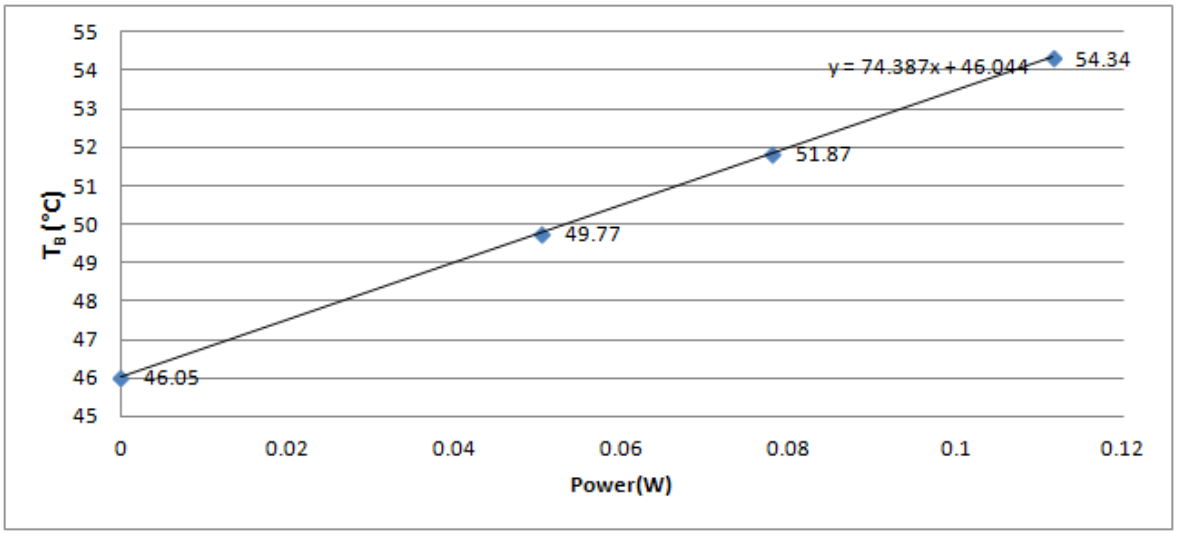

Figure 4.17. Power versus T_B graph of the system with P3HT film.

of the P3HT is calculated:

$$74.39 = \frac{W_{P3HT}\text{x}74.43}{W_{P3HT} + 74.43} \tag{4.30}$$

$$W_{P3HT} = 135000°C/W \tag{4.31}$$

The calculated W_{P3HT} is not precise enough even to determine the order of magnitude the thermal conductivity of the P3HT because as the thickness of the thin film reduces the thermal resistance of the sample increases and it becomes much bigger than the thermal resistance of the gap. If the thermal resistance of the gap can be reduced, $W_{leak} >> W_{sample}$ becomes invalid. Therefore surface area of the temperature sensors should be decreased. The thermal conductivity of the P3HT semiconducting polymer thin film for the estimated dimensions (1mm width, 1mm length,and 2μm thickness) and calculated thermal resistance is calculated:

$$135000 = \frac{1\text{x}10^{-3}}{\lambda_{P3HT}\text{x}2\text{x}10^{-6}\text{x}1\text{x}10^{-3}} \tag{4.32}$$

$$\lambda_{P3HT} = 3.703 W m^{-1} C^{-1} \tag{4.33}$$

As mentioned above the measurement result is far from the real thermal conductivity value. However, it can be said that the real value must be smaller than the measured value because as the thermal resistance decreases the system becomes more accurate. Since the figure of merit of thermoelectric materials increases with the decreasing thermal conductivity the results obtained from the experiment can put a lower limit for the figure of merit value.

The experimental setup is not sensitive enough to measure the thermal conductivity of a thin polymer film. 3-ω method, which is described in Section 4.1.1.1 uses micro structures for the measurement, is commonly used to measure the thermal conductivity of thin films and can be experienced [33, 39–42]. In addition to this, vertical thermal conductivity of P3HT thin film is measured using fiber aligned frequency domain thermoreflectance and is equal to 0.17 W/mK [43]. However, planar thermal conductivity of the P3HT thin film should be measured because of the anisotropy.

4.2. Electrical Conductivity

Electrical conductivity of the P3HT thin film is one of the main concerns of the thesis. Electrical conductivity of thin polymer films can be measured using four probe measurement. With the help of 4 point measurement, current and voltage electrodes are separated which eliminates the impedance contribution of the wiring and contact resistances [44]. Micro structures should be used to take contact from the polymer thin film.

Electrical conductivity of the P3HT is strongly depended on the doping level. Because activation energy increases with the increasing doping concentration which causes the electrical conductivity to increase. As a result, doping concentration of the polymer should be controlled to measure the electrical conductivity of the film. Xuan *et al.* doped the P3HT with $NOPF_6$ /acetonitrile solution for a prescribed time intervals

to dope it under control. The group made the measurements in the dark and under vacuum (1 x 10^{-6}Torr) to eliminate photooxidation [45] and they used a Keithley 2400 digital multimeter to utilize standard four probe measurement. The Figure 4.18 shows the doping level versus electrical conductivity graph of the P3HT.

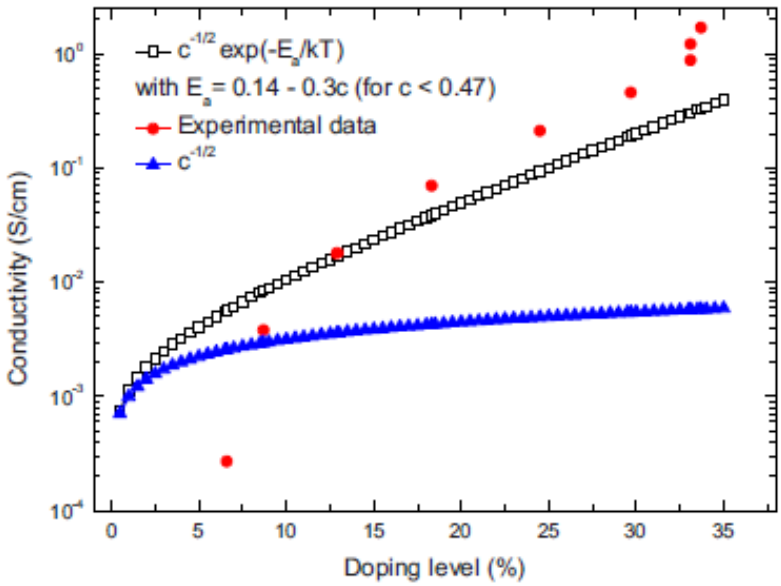

Figure 4.18. Doping level vs. electrical conductivity graph of the P3HT film [45].

As shown on the graph the electrical conductivity of the P3HT thin film polymer can vary between 10^{-2} and 10^{+2} S/m. The electrical conductivity of the P3HT thin film can be tuned in a inert environment by controlling the doping level, however; the carrier concentration also affects the other physical properties like thermal conductivity and Seebeck coefficient as mentioned in Section 3.3.

4.3. Seebeck Coefficient

The Seebeck coefficient can be measured by mounting a thin polymer film sample on a thermoelectric heater-cooler pair, with one electrode of the sample over one of the heater or cooler. Voltage difference caused by thermal energy and the temperature difference is measured with a source meter and a thermometer. Measurements are done for different temperature values and the slope of ΔV vs Δt plot is the Seebeck

coefficient. A material with a low Seebeck coefficient should be used compared to sample like copper for voltage leads to minimize the thermoelectric effect of the voltage leads [28].

Seebeck coefficient decreases with the increasing carrier density because the entropy change associated to adding a carrier is reduced as the density of sites already occupied by indistinguishable carrier rise. As a result Seebeck coefficient of P3HT should be measured for different doping concentrations. The Seebeck coefficient have already been measured for different doping concentrations. In the mentioned work two copper blocks separated are by a 5mm gap. The copper blocks was heated and the temperature are measured with K type thermocouples burried in the copper plates. The voltage difference was read with a high precision nanovoltmeter. The measurements are done in the dark and vacuum like the electrical conductivity measurement [45]. The obtained Seebeck coefficient vs doping level graph is shown in Figure 4.19.

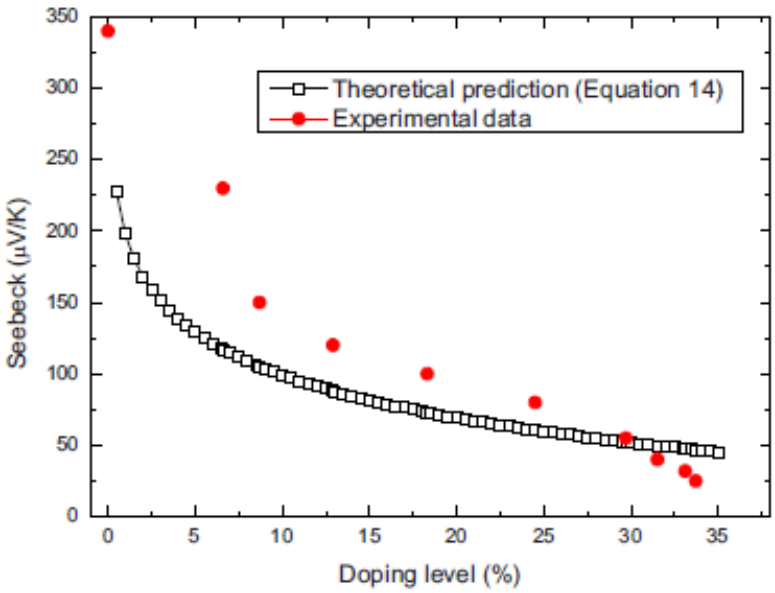

Figure 4.19. Doping level vs. Seebeck coefficient graph of the P3HT film [45].

As shown in the graph Seebeck coefficient decreases with the increasing doping level. To have a high thermoelectric figure of merit both the electrical conductivity and the Seebeck coefficient must be high. As a result power factor, which is the

numerator of the figure of merit and equals to $S^2\sigma$, reaches its maximum at a given doping level. Electrical conductivity vs Seebeck coefficient graph for different doping values is shown in Figure 4.20. The electrical power factor for doping levels between 21% and 31% reaches its maximum and equals to 1.4x10^{-7} $Wm^{-1}K^{-2}$. The power factor of the P3HT is low compared to the power factor of the Bi_2Te_3 which is equal to 2x10^{-4} $Wm^{-1}K^{-2}$.

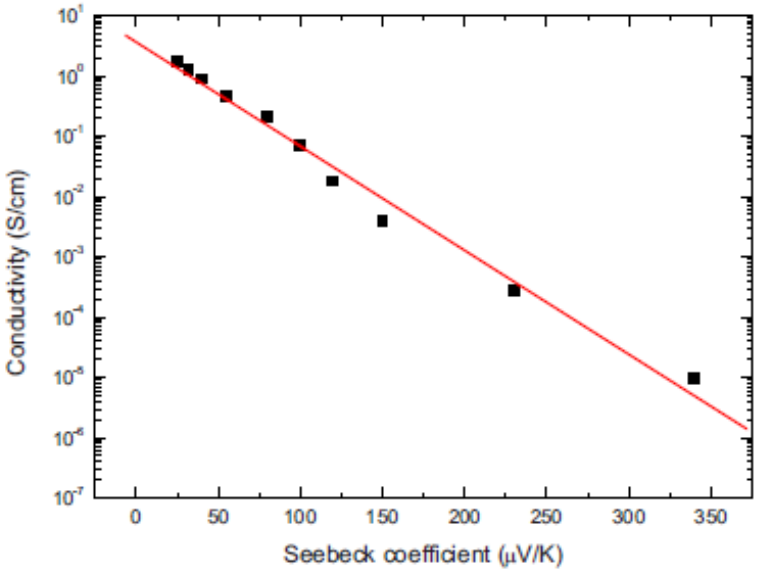

Figure 4.20. Electrical conductivity vs. Seebeck coefficient graph of the P3HT film [45].

To calculate the thermoelectric figure of merit of the P3HT at the given doping level, lateral thermal conductivity must be measured. However, we can use the measured vertical thermal conductivity measured with thermoreflectance method mentioned in Section 4.1.4.3. At the room temperature calculated ZT value for the given power factor and vertical thermal conductivity (with no knowledge of doping) is equal to 2.5 x 10^{-4}. The ZT value of P3HT is low compared to the materials mentioned in Section 3.3. However, P3HT still can be used in thermoelectric applications with some modifications like the PEDOT:PSS mentioned in Section 3.3.

5. CONCLUSION AND FUTURE WORK

The conclusion about the work done can be summarized as follows:

- The conducting and semiconducting polymers are promising thermoelectric materials because of their low cost due to abundance of carbon resources, easy synthesis, abundant electron energy bands through modulating, easy processing into versatile forms, high energy density, and low thermal conductivity.
- P3HT semiconducting polymer is a promising material for thermoelectric patterning because of its adjustable high electrical conductivity and low thermal conductivity.
- Thermoelectric figure of merit of P3HT can increased by adjusting the doping level and a value of 2.5 x 10^{-4} can be achieved.
- With a low cost experimental setup an opinion can be held about thermal conductivity of thin films and by decreasing the size of the experimental setup thermal conductivity can be measured with high accuracy.
- Thin film conducting and semiconducting polymers can be formed in vacuum to reduce the effects of air.

The future works that can be done to improve the results are listed:

- The size of the gap can be defined more accurately and finely with MEMS structures, input power can be increased, and the pressure of the chamber can be decreased to increase the accuracy and precision.In addition to this 3-ω method can be used to measure the thermal conductivity.
- Thermal resistances of films that have different lengths can be measured to remove the effect of contact thermal resistance.
- Thermal conductivity, electrical conductivity and Seebeck coefficient can be measured simultaneously for different temperatures and doping levels.
- Thermoelectric devices like thermocouple and peltier cooler can be designed to show the usage of conducting and semiconducting polymers in this area.

- Different conducting and semiconducting polymers and composites of polymers and inorganics can be researched to find materials with a higher thermoelectric figure of merit.
- Doping concentration of P3HT can be optimized to adjust thermal and electrical conductivity to use in thermal patterning applications.

REFERENCES

1. Lu, B., J. Xu, C. Fan, H. Miao and L. Shen, "Electrochemical Polymerization of Benzanthrone and Characterization of its Excellent Green-light-emitting Polymer", *The Journal of Physical Chemistry B*, Vol. 113, No. 1, pp. 37–48, 2009.

2. Bao-Yang, L., L. Cong-Cong, L. Shan, X. Jing-Kun, J. Feng-Xing, L. Yu-Zhen and Z. Zhuo, "Thermoelectric Performances of Free-Standing Polythiophene and Poly(3-Methylthiophene) Nanofilms", *Chinese Physics Letters*, Vol. 27, No. 5, 2010.

3. Bubnova, O., Z. U. Khan, A. Malti, S. Braun, M. Fahlman, M. Berggren and X. Crispin, "Optimization of the Thermoelectric Figure of Merit in the Conducting Polymer Poly(3,4-ethylenedioxythiophene)", *Nature Materials*, Vol. 10, No. 6, pp. 429–433, 2011.

4. Mutlu, S. and A. O. Sevim, "An Active Microheater Matrix Using Polymer Semiconductor Diodes for Thermal Patterning", *Journal of Micromechanics and Microengineering*, Vol. 20, No. 035019, pp. 1–8, 2010.

5. Becker, G., C. Lee and Z. Lin, *Thermal Conductivity in Advanced Chips*, 2005, `http://www.electroiq.com/articles/ap/print/volume-14/issue-7/features/cover-story/thermal-conductivity-in-advanced-chips.html`, accessed at Aug 2013.

6. Anthony, T. R., W. F. Banholzer, J. F. Fleischer, L. Wei, P. K. Kuo, R. L. Thomas and R. W. Pryor, "Thermal Diffusivity of Isotopically Enriched ^{12}C Diamond", *Phys. Rev. B*, Vol. 42, pp. 1104–1111, 1990.

7. Kaye, G. W. C. and T. H. Laby, *Tables of Physical and Chemical Constants*, Longman, London, UK, 1995.

8. Young, H., M. Zemansky and F. Sears, *University Physics*, Addison Wesley, Florida, USA, 1988.

9. Haynes, W., *CRC Handbook of Chemistry and Physics*, CRC Press, WV, USA, 2013.

10. James, A. and M. Lord, *MacMillan's Chemical and Physical Data*, Macmillan Press, Basingstoke, UK, 1992.

11. Jimison, L. H., M. F. Toney, I. McCulloch, M. Heeney and A. Salleo, "Charge-Transport Anisotropy Due to Grain Boundaries in Directionally Crystallized Thin Films of Regioregular Poly(3-hexylthiophene)", *Advanced Materials*, Vol. 21, No. 16, pp. 1568–1572, 2009.

12. Brinkmann, M. and J.-C. Wittmann, "Orientation of Regioregular Poly(3-hexylthiophene) by Directional Solidification: A Simple Method to Reveal the Semicrystalline Structure of a Conjugated Polymer", *Advanced Materials*, Vol. 18, No. 7, pp. 860–863, 2006.

13. Saini, V., Z. Li, S. Bourdo, E. Dervishi, Y. Xu, X. Ma, V. P. Kunets, G. J. Salamo, T. Viswanathan, A. R. Biris, D. Saini and A. S. Biris, "Electrical, Optical, and Morphological Properties of P3HT-MWNT Nanocomposites Prepared by in Situ Polymerization", *The Journal of Physical Chemistry C*, Vol. 113, No. 19, pp. 8023–8029, 2009.

14. Tanase, C., E. Meijer, P. Blom and D. de Leeuw, "Local Charge Carrier Mobility in Disordered Organic Field-Effect Transistors", *Organic Electronics*, Vol. 4, No. 1, pp. 33–37, 2003.

15. Xie, X., H. Ju and E.-C. Lee, "Band Gap Enhancement by Covalent Interactions in P3HT/PCBM Photovoltaic Heterojunction", *Journal of Korean Physical Society*, Vol. 57, p. 144, 2010.

16. Tanase, C., E. Meijer, P. Blom and D. de Leeuw, "Local Charge Carrier Mobility in Disordered Organic Field-Effect Transistors", *Organic Electronics*, Vol. 4, No. 1, pp. 33–37, 2003.

17. Worne, J., *Charge Transport and Transfer at the Nanoscale Between Metals and Novel Conjugated Materials*, Ph.D. Dissertation, Rice University, 2012.

18. Feng, X., G. Liu, S. Xu, H. Lin and X. Wang, "3-Dimensional Anisotropic Thermal Transport in Microscale Poly(3-hexylthiophene) Thin Films", *Polymer*, Vol. 54, No. 7, pp. 1887–1895, 2013.

19. Herlogsson, L., *Electrolyte-Gated Organic Thin-Film Transistors*, Ph.D. Dissertation, Linkoping Studies in Science and Technology, 2011.

20. Weber, E. H., *Development and Modeling of Thermally Conductive Polymer/Carbon Composites*, Ph.D. Dissertation, Michigan Technological University, 2001.

21. Tritt, T. M., *Thermal Conductivity: Theory, Properties, and Applications*, Kluwer Academic / Plenum Publishers, New York, USA, 2004.

22. Pichanusakorn, P. and P. Bandaru, "Nanostructured Thermoelectrics", *Materials Science and Engineering: R: Reports*, Vol. 67, No. 2–4, pp. 19–63, 2010.

23. Asheghi, M., K. Kurabayashi, R. Kasnavi and K. E. Goodson, "Thermal Conduction in Doped Single-Crystal Silicon Films", *Journal of Applied Physics*, Vol. 91, No. 8, pp. 5079–5088, 2002.

24. Rowe, D. M., *CRC Handbook of Thermoelectrics*, CRC Press, 1995.

25. Yue, R. and J. Xu, "Poly(3,4-ethylenedioxythiophene) as Promising Organic Thermoelectric Materials: A Mini-Review", *Synthetic Metals*, Vol. 162, No. 11–12, pp. 912–917, 2012.

26. Kong, F., C. Liu, J. Xu, Y. Huang, J. Wang and Z. Sun, "Thermoelectric Performance Enhancement of Poly(3,4-ethylenedioxythiophene):Poly(styrenesulfonate) Composite Films by Addition of Dimethyl Sulfoxide and Urea", *Journal of Electronic Materials*, Vol. 41, No. 9, pp. 2431–2438, 2012.

27. Song, H., C. Liu, H. Zhu, F. Kong, B. Lu, J. Xu, J. Wang and F. Zhao, "Improved Thermoelectric Performance of Free-Standing PEDOT:PSS/Bi2Te3 Films with Low Thermal Conductivity", *Journal of Electronic Materials*, Vol. 42, No. 6, pp. 1268–1274, 2013.

28. Zhang, B., J. Sun, H. E. Katz, F. Fang and R. L. Opila, "Promising Thermoelectric Properties of Commercial PEDOT:PSS Materials and Their Bi2Te3 Powder Composites", *ACS Applied Materials & Interfaces*, Vol. 2, No. 11, pp. 3170–3178, 2010.

29. Gubler, U., M. Raunhardt and A. Stump, "Measurement Technique for Thermal Conductivity of Thin Polymer Films", *Thin Solid Films*, Vol. 515, No. 4, pp. 1737–1740, 2006.

30. Wang, H. and M. Sen, "Analysis of the 3-ω method for thermal conductivity measurement", *International Journal of Heat and Mass Transfer*, Vol. 52, No. 7–8, pp. 2102 – 2109, 2009.

31. Cahill, D. G., "Thermal Conductivity Measurement from 30 to 750 K: The 3 Omega Method", *Review of Scientific Instruments*, Vol. 61, No. 2, pp. 802–808, 1990.

32. Moon, I. K., Y. H. Jeong and S. I. Kwun, "The 3 Omega Technique for Measuring Dynamic Specific Heat and Thermal Conductivity of a Liquid or Solid", *Review of Scientific Instruments*, Vol. 67, No. 1, pp. 29–35, 1996.

33. Fagani, F., *Thermal Conductivity Measurement of PEDOT:PSS by 3-Omega Technique*, M.Sc. Thesis, Linkoping Studies in Science and Technology, 2010.

34. Cahill, D. G. and R. O. Pohl, "Thermal Conductivity of Amorphous Solids Above the Plateau", *Phys. Rev. B*, Vol. 35, pp. 4067–4073, 1987.

35. Inc., F. S., *Thermal Analysis of Semiconductor Systems*, 2008, `http://www.freescale.com/files/analog/doc/white_paper/BasicThermalWP.pdf`, accessed at June 2013.

36. Rohsenow, W. and J. Hartnett, *Handbook of Heat Transfer*, McGraw Hill Book Company, New York, USA, 1973.

37. Incroper, F., D. Dewitt, T. Bergman and A. Lavine, *Introduction to Heat Transfer*, John Wiley & Sons Inc., New Jersey, USA, 2007.

38. Cryotronics, L. S., *DIN IEC 751 Temperature/Resistance Table for Platinum Sensors*, 2000, `http://www.lakeshore.com/Documents/F038-00-00.pdf`, accesed at Aug 2013.

39. Kaul, P. B., K. A. Day and A. R. Abramson, "Application of the Three Omega Method for the Thermal Conductivity Measurement of Polyaniline", *Journal of Applied Physics*, Vol. 101, No. 8, 2007.

40. Abramson, A., W. C. Kim, S. Huxtable, H. Yan, Y. Wu, A. Majumdar, C.-L. Tien and P. Yang, "Fabrication and Characterization of a Nanowire/Polymer-Based Nanocomposite for a Prototype Thermoelectric Device", *Microelectromechanical Systems, Journal of*, Vol. 13, No. 3, pp. 505–513, 2004.

41. Jin, J., M. P. Manoharan, Q. Wang and M. A. Haque, "In-Plane Thermal Conductivity of Nanoscale Polyaniline Thin Films", *Applied Physics Letters*, Vol. 95, No. 3, 2009.

42. Sun, J., M.-L. Yeh, B. J. Jung, B. Zhang, J. Feser, A. Majumdar and H. E. Katz, "Simultaneous Increase in Seebeck Coefficient and Conductivity in a Doped Poly(alkylthiophene) Blend with Defined Density of States", *Macromolecules*,

Vol. 43, No. 6, pp. 2897–2903, 2010.

43. Malen, J. A., K. Bahetti, T. Tong, J. A. Hudgings, A. Majumdar and Y. Zhao, "Optical Measurement of Thermal Conductivity Using Fiber Aligned Frequency Domain Thermoreflectance", *Journal of Heat Transfer*, Vol. 133, No. 8, 2011.

44. Fransilla, S., *Introduction to Microfabrication*, John Wiley & Sons, New York, USA, 2010.

45. Xuan, Y., X. Liu, S. Desbief, P. Leclère, M. Fahlman, R. Lazzaroni, M. Berggren, J. Cornil, D. Emin and X. Crispin, "Thermoelectric Properties of Conducting Polymers: The Case of Poly(3-hexylthiophene)", *Phys. Rev. B*, Vol. 82, 2010.